GEOLOGICAL SURVEY OF CANADA
OPEN FILE 7582

Targeted Geoscience Initiative 4: Contributions to the Understanding of Precambrian Lode Gold Deposits and Implications for Exploration

Geological setting of the world-class Musselwhite gold mine, Superior Province, northwestern Ontario: implications for exploration

William Oswald[1], Sébastien Castonguay[2], Benoît Dubé[2], Vicki J. McNicoll[3], John Biczok[4], Michel Malo[1], and Patrick Mercier-Langevin[2]

[1]Institut national de la recherche scientifique – Centre Eau Terre Environnement, Québec, Quebec
[2]Geological Survey of Canada, Québec, Quebec
[3]Geological Survey of Canada, Ottawa, Ontario
[4]Goldcorp Inc., Thunder Bay, Ontario

2015

This publication is available for free download through GEOSCAN (http://geoscan.nrcan.gc.ca/)

Recommended citation

Oswald, W., Castonguay, S., Dubé, B., McNicoll, V.J., Biczok, J., Malo, M., and Mercier-Langevin, P., 2015. Geological setting of the world-class Musselwhite gold mine, Superior Province, northwestern Ontario: implications for exploration, *In:* Targeted Geoscience Initiative 4: Contributions to the Understanding of Precambrian Lode Gold Deposits and Implications for Exploration, (ed.) B. Dubé and P. Mercier-Langevin; Geological Survey of Canada, Open File 7582, p. 69–84.

Publications in this series have not been edited; they are released as submitted by the author.

Contribution to the Geological Survey of Canada's Targeted Geoscience Initiative 4 (TGI-4) Program (2010–2015)

TABLE OF CONTENTS

Geological setting of the world-class Musselwhite gold mine, Superior Province, northwestern Ontario: implications for exploration

William Oswald[1*], Sébastien Castonguay[2†], Benoît Dubé[2], Vicki J. McNicoll[3], John Biczok[4], Michel Malo[1], and Patrick Mercier-Langevin[2]

[1]Institut national de la recherche scientifique – Centre Eau Terre Environnement, 490 rue de la Couronne, Québec, Quebec G1K 9A9
[2]Geological Survey of Canada, 490 rue de la Couronne, Québec, Quebec G1K 9A9
[3]Geological Survey of Canada, 601 Booth Street, Ottawa, Ontario K1A 0E8
[4]Goldcorp Inc., Musselwhite Mine, Thunder Bay, Ontario P7B 6S8
*Corresponding author's e-mail: william.oswald@ete.inrs.ca
†Corresponding author's e-mail: sebastien.castonguay@RNCan-NRCan.gc.ca

ABSTRACT

The Musselwhite world-class Au deposit is hosted in polydeformed amphibolite-facies banded iron formation of the Opapimiskan-Markop metavolcanic assemblage, part of the Mesoarchean North Caribou greenstone belt (northwestern Superior Province). The deposit is located approximately 2 km west of the tectonic boundary with the gneissic Island Lake Domain. Major and trace element geochemical data show that the South Rim and Opapimiskan-Markop metavolcanic assemblages have variable magmatic affinities and diverse normalized rare earth element patterns. The bulk of the Au at Musselwhite is hosted in silicate-rich banded iron formation and occurs in association with stratabound pyrrhotite replacements and associated silica flooding, with local discordant quartz±pyrrhotite veins. The ore zones are associated with D_2 high-strain zones that are preferentially developed along hinges and strongly attenuated fold limbs of tight F_2 folds. The layered anisotropy induced by the presence of competent banded iron formation layers in mafic and ultramafic volcanic rocks has clearly influenced the rheological response to deformation at all scales, and hence played an important role in Au-bearing fluid flow and ore formation and distribution. A new U-Pb preliminary age of 2666 Ma on late-M_2 monazite provides a minimum age constraint for the regional D_2 metamorphic/deformation event to which most of the Au mineralization at Musselwhite is associated. Reappraisal of stratigraphic relationships, supported by U-Pb geochronology, indicates that the mine stratigraphy is inverted and is part of the overturned limb of a kilometre-scale F_1 syncline, which is in agreement with multiple occurrences of mesoscopic refolded F_1 folds. Previously unrecognized regional F_1 folding, which is strongly overprinted by the dominant D_2 deformation, has influenced the distribution and geometry of the banded iron formation, which hosts the bulk of the Au at Musselwhite, and provides new vectors for regional exploration. Future work will focus on additional documentation of mineral chemistry and microscopic textural relationships, as well as further analyses of lithogeochemical data in order to ultimately define key exploration vectors for iron formation-hosted Au deposits in other Precambrian terranes.

INTRODUCTION

The Goldcorp Musselwhite mine is located near Opapimiskan Lake, 475 km north of Thunder Bay, within the North Caribou greenstone belt, which is part of the North Caribou Terrane of the western Superior Province (Thurston et al., 1991; Fig. 1). Production started in 1997 and had reached over 4 Moz of gold with total proven and probable reserves of 1.85 Moz as of December 31, 2013 (www.goldcorp.com).

This research project at Musselwhite, a component of the Targeted Geoscience Initiative 4 (TGI-4) Lode Gold project of Natural Resources Canada, is conducted in collaboration with Goldcorp Inc., the Ontario Geological Survey and the University of Ottawa. It aims at understanding the structural, lithological, and geochemical controls on the formation and distribution of the banded iron formation-hosted Au mineralization. Another objective is to define the geochemical footprint of the hydrothermal system in order to develop improved geological and exploration models for similar deposit types in the North Caribou greenstone belt and elsewhere in Precambrian terranes (Dubé et al., 2011).

Oswald, W., Castonguay, S., Dubé, B., McNicoll, V.J., Biczok, J., Malo, M., and Mercier-Langevin, P., 2015. Geological setting of the world-class Musselwhite gold mine, Superior Province, northwestern Ontario: implications for exploration, *In:* Targeted Geoscience Initiative 4: Contributions to the Understanding of Precambrian Lode Gold Deposits and Implications for Exploration, (ed.) B. Dubé and P. Mercier-Langevin; Geological Survey of Canada, Open File 7582, p. 69–84.

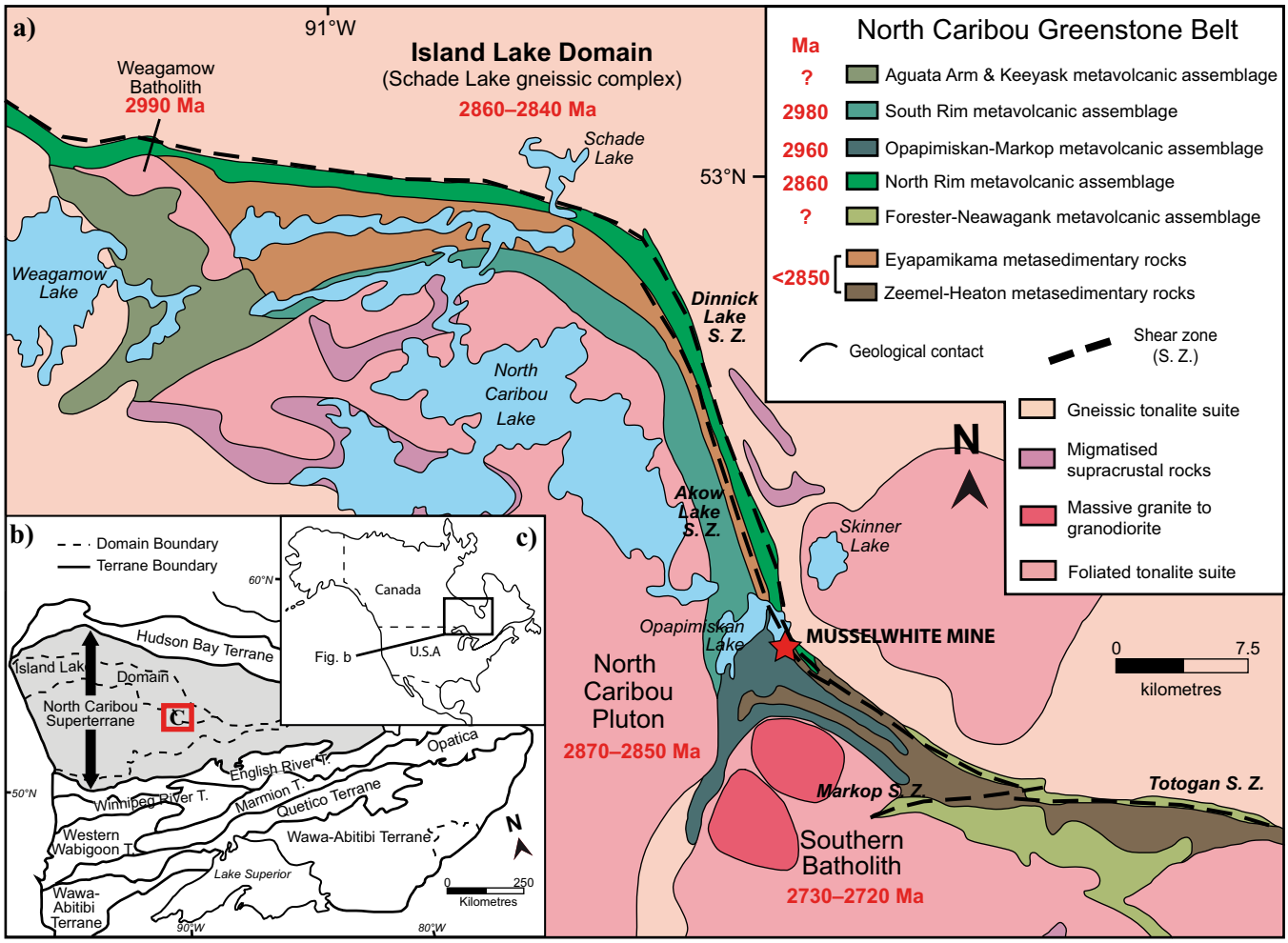

Figure 1. a) Simplified tectonostratigraphic map of the North Caribou greenstone belt and surrounding area (geology modified from McNicoll et al., 2013; geochronological data from Breaks, 2001; McNicoll et al., 2013; Van Lankvelt, 2013). **b and c)** Location of the study area and terranes of the western Superior Province (insets modified from Rayner and Stott, 2005; Stott et al., 2010).

This report presents a brief summary of the current status of the ongoing multidisciplinary research being conducted at Musselwhite. Our investigation of the distal and proximal settings of Au mineralization and of the relative and absolute chronology of events at Musselwhite comprises a major surface, underground, and drill-core mapping component, including sampling for petrographic and geochemical analyses. The study of the Musselwhite deposit (Oswald et al., 2014a,b), which builds on previous studies at deposit scale (e.g. Hall and Rigg, 1986; Couture, 1995; Isaac, 2008; Moran, 2008), also includes targeted geochronology across most of the Opapimiskan Lake area (McNicoll et al., 2013, submitted) to establish the age of the host-rock successions and the major structural and metamorphic episodes, to put our work into a regional context, and to address key questions that cannot be readily resolved at deposit scale. Other specific ongoing research activities at Musselwhite or its vicinity (e.g. Kalbfleisch, 2012; Van Lankvelt et al., 2013; Duff, 2014; Gourcerol et al., 2015) involve geochronology, structural mapping, metamorphic petrology, and lithogeochemistry, which will collectively contribute to a better understanding of the evolution of the North Caribou greenstone belt and its bounding structures and assemblages.

REGIONAL AND LOCAL GEOLOGICAL SETTING

The North Caribou greenstone belt is located south-southwest of the Island Lake domain (Fig. 1), in the central part of the North Caribou Terrane, which is considered the core of the western Superior Province (Percival et al., 2007). Regional-scale mapping programs and studies (Breaks et al., 1985; Piroshco et al., 1989; Breaks and Barlett, 1991; Breaks et al., 1991, 2001; Thurston et al., 1991) have defined various lithostratigraphic assemblages in the North Caribou greenstone belt (from northwest to southeast; Fig. 1a): the Agutua Arm metavolcanic assemblage; the

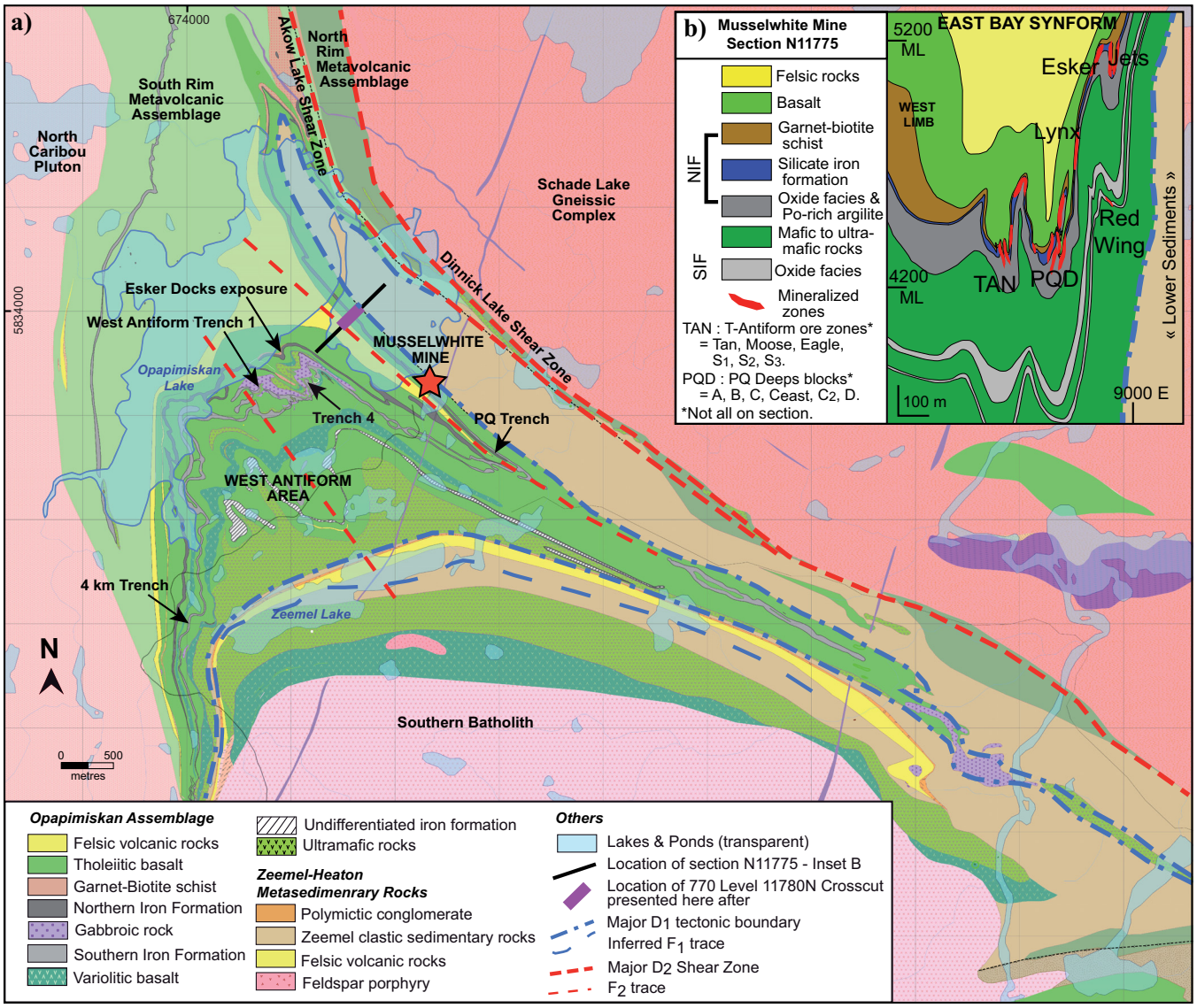

Figure 2. a) Geological map of the Opapimiskan Lake area and major structural features, with locations of the surface exposures that were selected for detailed mapping for this project (geology based on unpublished Goldcorp data). Universal Transverse Mercator (UTM) co-ordinates provided using North American Datum 1983 (NAD83) in Zone 15. **b)** Simplified geological section of the mine at N11775 mine grid, showing the locations of the main ore zones. Abbreviations: bt = biotite; gt = garnet; ML = mine level; NIF = Northern Iron Formation; po = pyrrhotite; SIF = Southern Iron Formation.

metasedimentary and metavolcanic rocks of the Keeyask metavolcanic assemblage; the metasedimentary rocks of the Eyapamikama assemblage; the North Rim metavolcanic assemblage; the South Rim metavolcanic assemblage; the Opapimiskan-Markop metavolcanic assemblage (OMA); the Zeemel-Heaton metasedimentary assemblage (ZHA); and the Forester-Neawagank metavolcanic assemblage. The greenstone belt is surrounded by the tonalite-trondhjemite-granodiorite (TTG)-type batholiths of the North Caribou pluton (NCP) and the Schade Lake gneissic complex (SLGC), both comprising several intrusive phases dated between 2.87 and 2.84 Ga, and by the smaller, composite, ca. 2730–2723 Ma Southern batholith (Fig. 1; Biczok et al., 2012).

The Musselwhite deposit host succession consists of the South Rim metavolcanic assemblage and the underlying OMA, which structurally overlies the ZHA (Fig. 2a). The whole succession is folded by a northwest-trending, F_2 synform-antiform pair (i.e. East Bay Synform and West Antiform). The OMA comprises two main iron formations, i.e., the Northern iron formation (NIF) and Southern iron formation (SIF), both intercalated with, from structural top to bottom, calc-alkaline, felsic to intermediate volcanic rocks, tholeiitic, mafic volcanic and subvolcanic rocks, and tholeiitic, komatiitic basalt and ultramafic volcanic rocks. The structurally uppermost iron formation sequence (NIF) hosts the bulk of the economic Au mineralization (Fig. 2b).

Three main phases of regional deformation have been documented (Breaks et al., 1985, 1991; Piroshco and Shields, 1985) The earliest event, D_1, consists of tight to isoclinal mesoscopic folds, associated with a penetrative S_1 foliation, which is commonly subparallel to bedding or layering (Breaks et al., 2001). D_2, the dominant regional phase of deformation, consists of open to isoclinal shallowly northwest-plunging folds, coupled with a steeply dipping axial-planar foliation (S_2), commonly obliterating D_1 fabrics. In the project area, rocks are affected by strong, eastward-increasing D_2 deformation that culminates in a major fault zone at the contact with the Schade Lake gneissic complex (Fig. 2a). D_3 deformation structures are heterogeneously developed and consist of asymmetric broad open or chevron folds, locally accompanied by a steep southwest-trending S_3 crenulation cleavage. Major, probably long-lived or reactivated fault or shear zones commonly mark lithostratigraphic boundaries in the greenstone belt and overprint contacts with surrounding batholiths (Figs. 1, 2; Breaks et al., 2001).

The regional metamorphic grade varies from middle to upper greenschist facies in the northern part of the belt, near Eyapamikama Lake (Breaks and Bartlett, 1991), to middle amphibolite facies around Opapimiskan Lake and further east (Breaks et al., 1985). According to Hall and Rigg (1986), peak regional metamorphism occurred during the later stages of D_2.

RESULTS

Methodology

Detailed geological and structural mapping was carried out using a high-resolution GPS (AshTech Promark 800) on a selection of five stripped exposures, which allowed for increased speed of data collection as well as overcoming the challenge of structural measurements on iron formations. This latter issue was resolved during underground mapping by measuring fabrics and structures with respect to the surveyed orientation of mine workings. Systematic logging and sampling of drill core has also been completed on a set of sections across the deposit to link geological and structural mapping information with petrographic data, mineral chemistry, and whole-rock lithogeochemistry.

Mine Stratigraphy

Geological mapping (Fig. 3; see also Oswald et al., 2014a,b), description of drill core, and lithogeochemical data have refined the stratigraphy of the deposit (Fig 4). Previously defined units of the Opapimiskan metavolcanic assemblage (Fig. 4a; Hollings and Kerrich, 1999) have been geochemically characterized. Volcanic rocks from the "Avol" are dominantly dacitic with a calc-alkaline affinity (Fig. 4b,c). The "Bvol" package comprises tholeiitic mafic rocks with three contrasting rare earth element (REE) signatures: one with light REE enrichment and two flat-profile groups with different REE enrichment relative to primitive mantle values (Fig. 4d). The "Basement Basalts" contain ultramafic rocks with a transitional to calc-alkaline affinity and light REE enrichment, intercalated with ultramafic rocks of tholeiitic affinity and flat normalized REE patterns, calc-alkaline intermediate rocks showing strong light REE enrichment, and tholeiitic to slightly calc-alkaline mafic rocks showing various degrees of light REE enrichment. Four samples of basalt and komatiitic basalt of the lowermost section of the OMA were collected close to the boundary with the ZHA (Fig. 2a); they have tholeiitic affinity and exhibit flat normalized REE patterns.

The NIF comprises garnet amphibolite and garnet-biotite schist (unit 4E and 4F, Fig. 4a), which, although not banded iron formation *sensu stricto*, contain over 15 wt% total Fe_2O_3 (Fig. 4d) and are thereby considered iron formation (James, 1954). Unit 4F includes a thin quartz-feldspar-biotite volcaniclastic interval (unit 6). These units structurally overlie the more typical banded iron formation, including a silicate (i.e. garnet-grunerite) facies (unit 4EA), a clastic chert-magnetite facies (unit 4Bc), a chert-magnetite facies (unit 4B), and a chert-grunerite facies (unit 4A). A sulphide-rich meta-argillite (unit 4H) forms the structural base of the NIF sequence (Fig. 4a). The Al_2O_3 content of samples is used in ternary projections (Fig. 4e) as a proxy for detrital input (Klein, 2005); the hydrothermal input is mainly defined by a positive Eu anomaly, whereas a weakly to strongly positive Y anomaly characterizes the seawater input (Fig. 4f). Following Moran (2008), REE+Y data was chondrite (C1)-normalized and was also normalized to the mudstone of Queensland (MUQ; Kamber et al., 2005; Fig. 4f) to minimize the detrital REE signature and to emphasize potential hydrothermal and seawater inputs (Baldwin, 2011).

The study of the chert component of the iron formations at Musselwhite and in other BIF-hosted deposits (e.g. Meadowbank Mine, and Meliadine district, Nunavut) by Gourcerol et al. (2014, 2015), which is complementary to our work, aims to establish if there is specific geochemical signature for BIF that contains Au mineralization and whether a hydrothermal footprint can be detected.

Structure

Complementing the work of Hall and Rigg (1986) 2 to 3 km west of the Musselwhite Mine, our surface and underground mapping has documented structures and fabrics related to the three phases of regional deformation and provides comprehensive insights about polyphase structural styles and geometric relationships

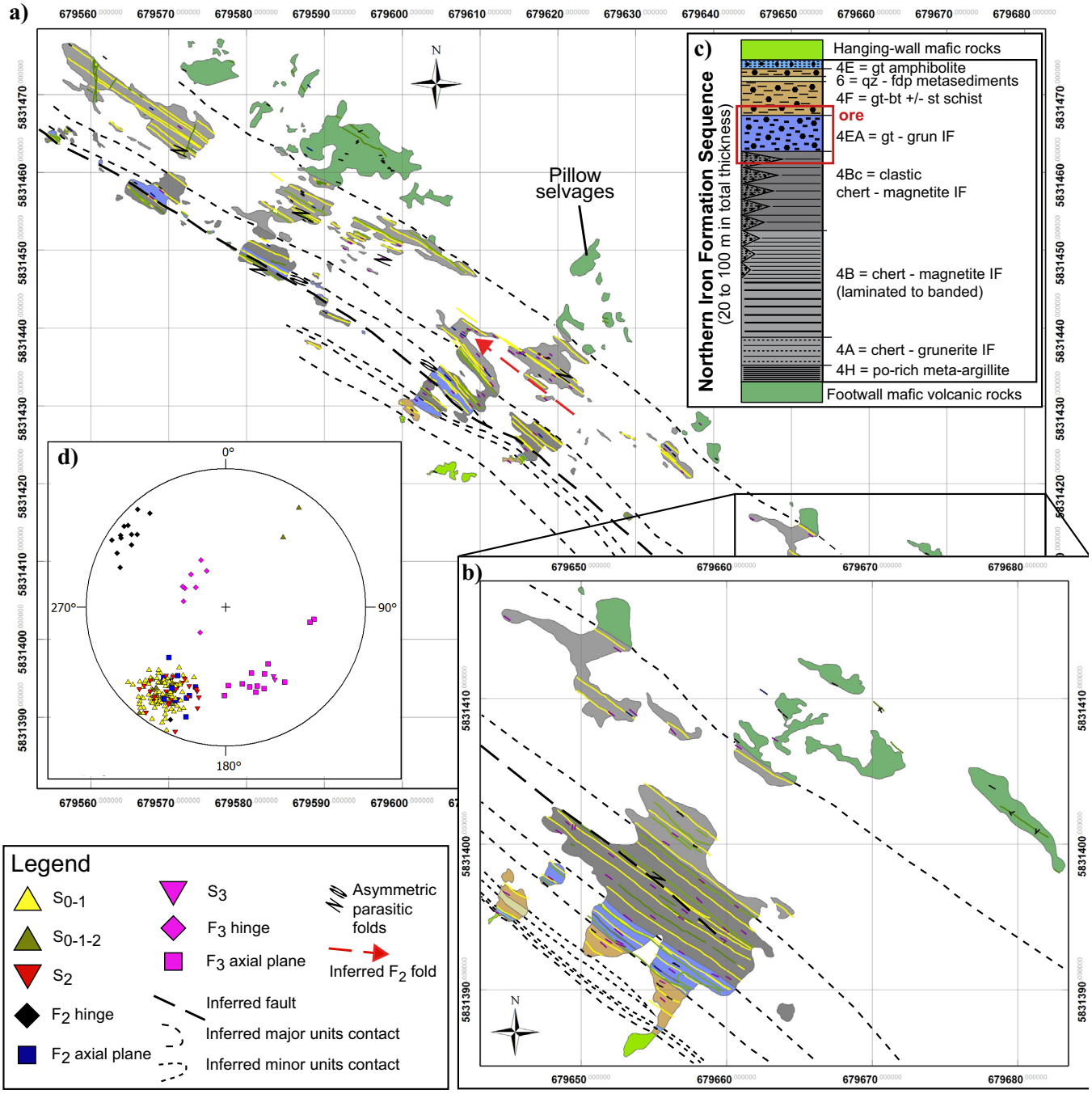

Figure 3. a) Geological map of the PQ Trench exposure (see Fig. 2 for location). **b)** Close-up view of the southern part of the exposure, UTM NAD83 Zone 15 coordinates. **c)** Schematic column of the facies of the Northern Iron Formation and adjacent volcanic rocks (based on unpublished Goldcorp data). Abbreviations: bt = biotite; fdp = feldspar; grun = grunerite; gt = garnet; IF = iron formation; po = pyrrhotite; qz = quartz; st = staurolite. **d)** Stereographic projection (lower hemisphere) of planar and linear structural data.

and their significance for gold mineralization (Oswald et al., 2014a,b,c). The West Antiform Trench 1, Esker Docks exposure, and Trench 4 are located in a domain of lower intensity D_2 deformation, which provides a favourable context to document earlier structures that include penetrative, northeast-southwest-trending, S_1 foliation (Fig. 5a), refolded F_1 folds (Fig. 5b), and locally, evidence of soft-sediment deformation. Shallowly northwest-plunging upright F_2 folds have deformed D_1 structures and produced type 3 F_1/ F_2 fold interference pattern in the West Antiform area. The expression of the axial-planar northwest-trending S_2 foliation is lithology-dependent (Fig. 5c). In a relatively low-intensity D_2 deformation domain, it is developed as a spaced cleavage in igneous rocks and as a more penetrative foliation in iron formation. In areas

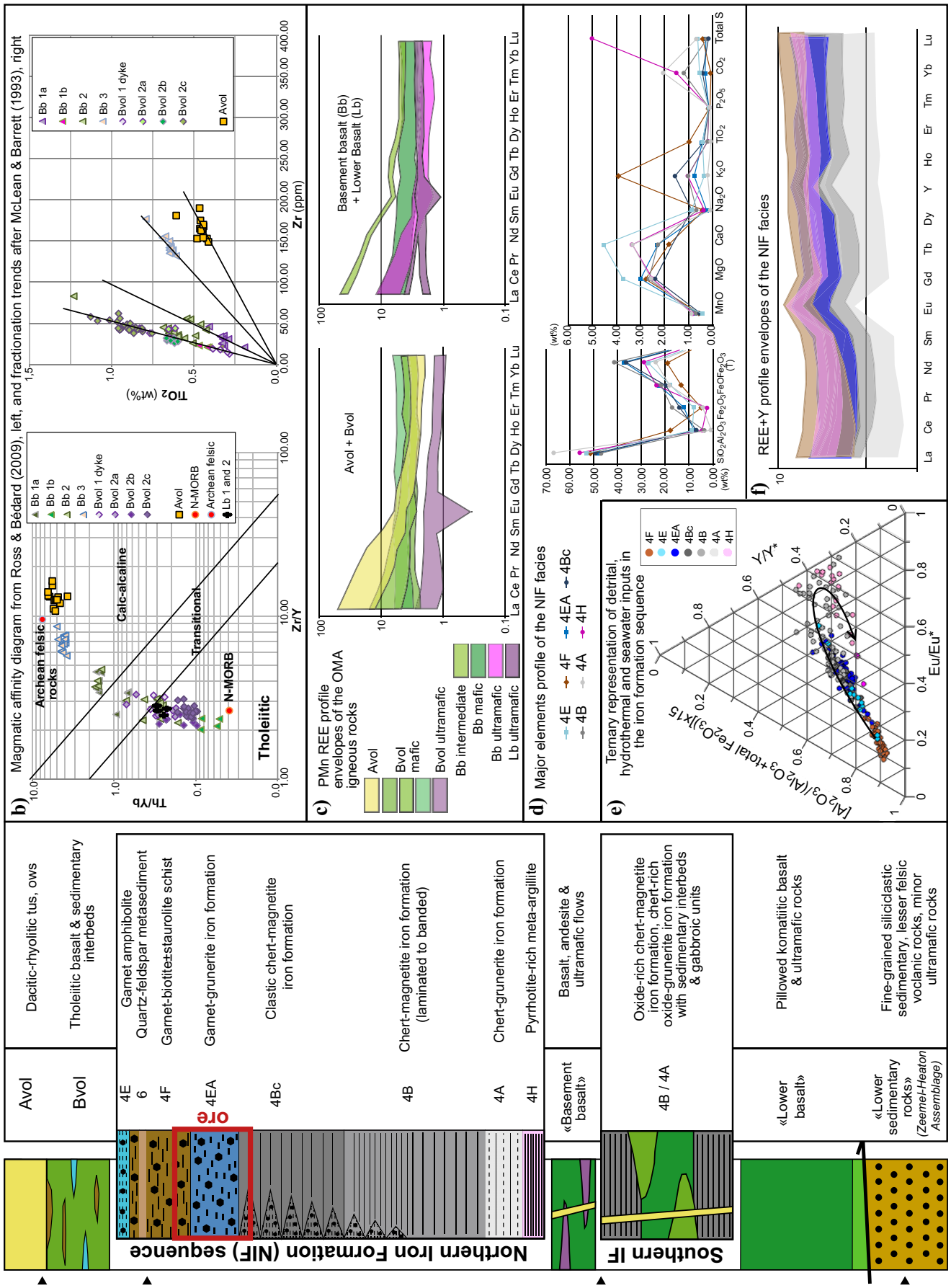
a)
2978,7 Ma
<2967 Ma
Felsic dyke: 2909,4 Ma
<2853 Ma
Avol
Bvol
Dacitic-rhyolitic tus, ows
Tholeiitic basalt & sedimentary interbeds
Garnet amphibolite
Quartz-feldspar metasediment
Garnet-biotite±staurolite schist
Garnet-grunerite iron formation
Clastic chert-magnetite iron formation
Chert-magnetite iron formation (laminated to banded)
Chert-grunerite iron formation
Pyrrhotite-rich meta-argillite
Basalt, andesite & ultramafic flows
Oxide-rich chert-magnetite iron formation, chert-rich oxide-grunerite iron formation with sedimentary interbeds & gabbroic units
Pillowed komatiitic basalt & ultramafic rocks
Fine-grained siliciclastic sedimentary, lesser felsic volcanic rocks, minor ultramafic rocks
4E
6
4F
4EA
4Bc
4B
4A
4H
ore
«Basement basalt»
4B / 4A
«Lower basalt»
«Lower sedimentary rocks» (Zeemel-Heaton Assemblage)
Northern Iron Formation (NIF) sequence
Southern IF
b)
Magmatic affinity diagram from Ross & Bédard (2009), left, and fractionation trends after McLean & Barrett (1993), right
Th/Yb
ZrY
Archean felsic rocks
Calc-alcaline
Transitional
N-MORB
Tholeiitic
Bb 1a
Bb 1b
Bb 2
Bb 3
Bvol 1 dyke
Bvol 2a
Bvol 2b
Bvol 2c
Avol
N-MORB
Archean felsic
Lb 1 and 2
TiO2 (wt%)
Zr (ppm)
c)
PMn REE profile envelopes of the OMA igneous rocks
Avol
Bvol mafic
Bvol ultramafic
Bb intermediate
Bb mafic
Bb ultramafic
Lb ultramafic
Avol + Bvol
Basement basalt (Bb) + Lower Basalt (Lb)
La Ce Pr Nd Sm Eu Gd Tb Dy Ho Er Tm Yb Lu
d)
Major elements profile of the NIF facies
4E
4F
4EA
4Bc
4B
4A
4H
(wt%)
MnO MgO CaO Na2O K2O TiO2 P2O5 CO2 Total S
SiO2-Al2O3-Fe2O3-FeO-Fe3O4 (T)
e)
Ternary representation of detrital, hydrothermal and seawater inputs in the iron formation sequence
[Al2O3/(Al2O3+total Fe2O3)]x15
Y/Y*
Eu/Eu*
f)
REE+Y profile envelopes of the NIF facies
La Ce Pr Nd Sm Eu Gd Tb Dy Y Ho Er Tm Yb Lu

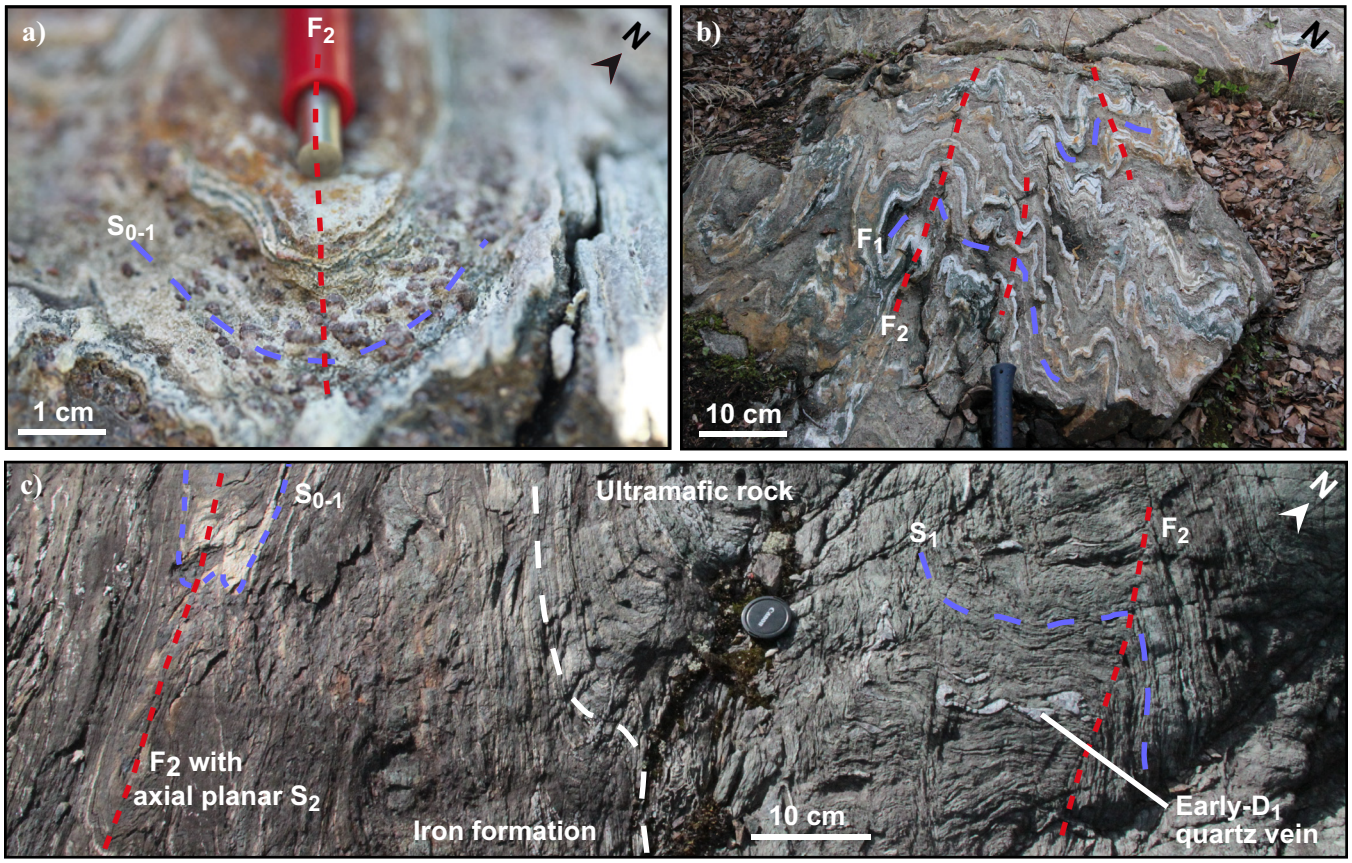

Figure 5. Photographs of representative structural features. **a)** Close-up view of the S_1 foliation in a garnet-biotite band along a F_2 fold hinge (Esker Docks exposure). **b)** F_1/F_2 fold interference pattern (type 3) in cherty garnet-biotite schist (Esker Docks exposure). **c)** Part of the West Antiform exposure illustrating the contrast in the development of the S_1 foliation in the chert-magnetite iron formation and the adjacent ultramafic rocks, overprinted by F_2 folds.

of strong D_2 overprint, S_2 is penetrative in all rock types and is associated with boudinaged beds in chert-magnetite iron formation. Strain features suggest that D_2 deformation in the mine area was dominated by flattening and minor shearing with dextral and east-side-up components of motion. D_3 deformation mostly consists of open or chevron-type folds. Two possibly conjugate sets of S_3 crenulation cleavage are oriented ENE-WSW and NNE-SSW. Field evidence reveals that S_3 cleavage is unevenly developed in the BIF units, and it is preferentially developed near and within high-strain zones in volcanic rocks.

Mineralization and Alteration

The crosscutting relationships of multiple vein generations are documented here. The earliest vein type includes barren, glassy, white to grey, quartz veins, which are thought to be early-D_1 (Fig. 5c). Three vein types are associated with D_2 structures: 1) grey, quartz-dominated, pyrrhotite- and carbonate-bearing, auriferous veins with a variably developed calc-silicate alteration halo; 2) milky white quartz-carbonate veins that can be auriferous or barren; and 3) barren, sugary-textured, calcite-dominated, quartz-carbonate late-D_2 veins. D_3-related veins, which are usually barren, white to greyish, and quartz-dominated, remobilized Au and sulphides locally where they cut pre-existing mineralized structures.

Characteristics of the mineralized zones have been documented by logging of drill core and underground mapping (Oswald et al., 2014a). As previously proposed for the West Antiform zone by Hall and Rigg

Figure 4 (opposite page). a) Detailed stratigraphic column of the mine sequence (geochronological data from McNicoll et al. (2013)). **b)** Left plot: magmatic affinity diagram from Ross and Bédard (2009) using Zr/Y versus Th/Yb, and right plot: fractionation trends after McLean and Barrett (1993) using Zr versus TiO_2 for the least altered drill-core samples. **c)** Rare earth element (REE) profile envelopes of igneous rocks samples from the mine sequence (normalized to primitive mantle from Sun and McDonough, 1989). **d)** Average values for major elements of the least altered drill-core samples of each Northern Iron Formation (NIF) facies. **e)** Ternary projection of NIF drill-core samples showing the relative importance of detrital input ($Al_2O_3/(A_2O_3$+total $Fe_2O_3)$x15), hydrothermal input (Eu anomaly), and seawater input (Y anomaly) for each facies. Black arrow shows the overall trend. **f)** Mudstone of Queensland (MUQ)-normalized REE+Y profile envelopes of the least altered drill-core samples of each NIF facies (normalized to MUQ from Kamber et al., 2005). See Figure 4e for colour legend.

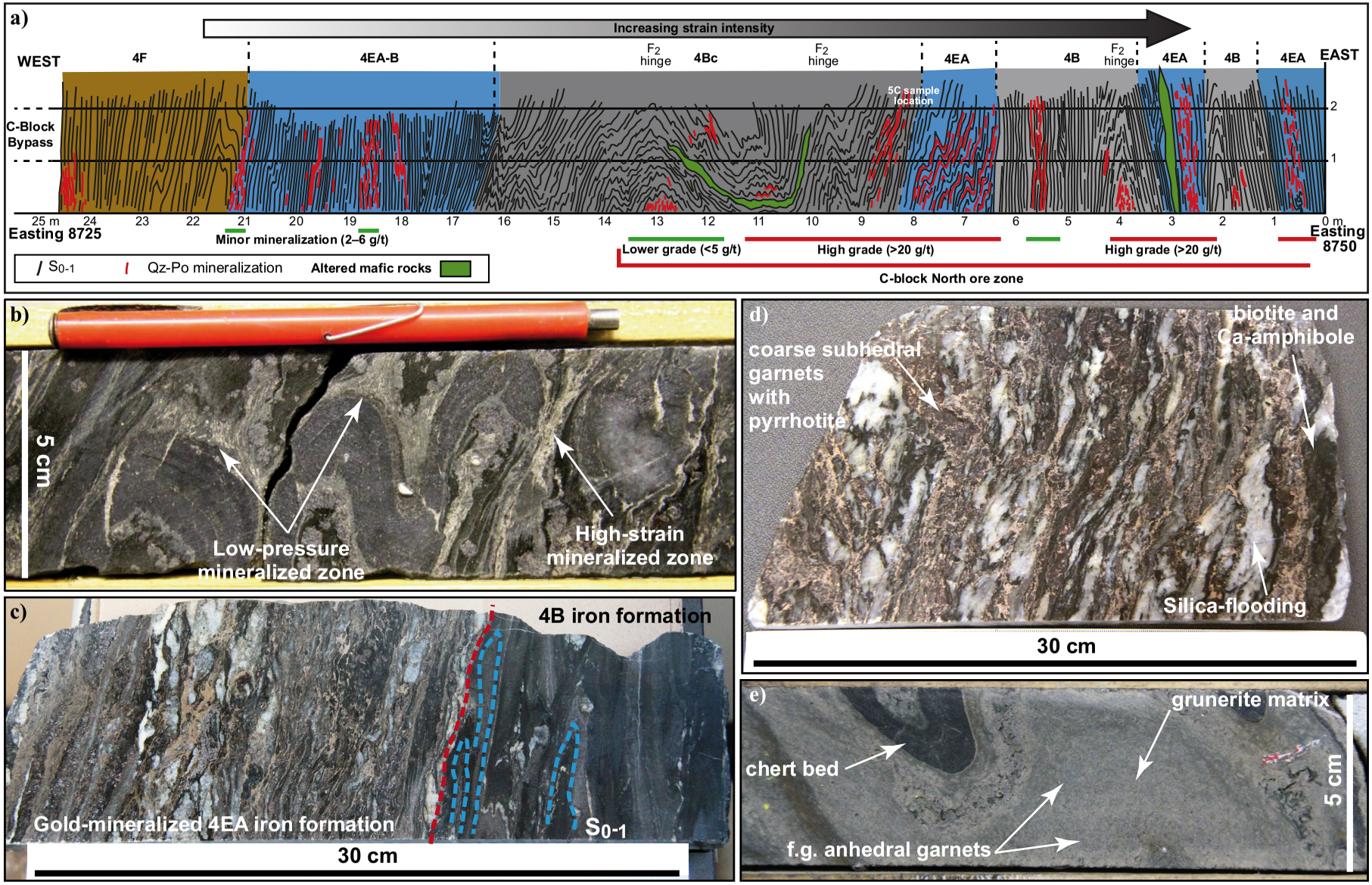

Figure 6. a) Geology of the northern wall of the 770 Level 11780N Crosscut (see Fig. 3a for colour legend). **b)** Photograph of drill core (sample MW-2011-107) showing the style and distribution of the mineralization, which is similar to those mapped on the 770 Level 11780N crosscut face. **c)** Photograph of a polished slab of ore sampled on the north-facing wall of the 770 Level 11780N Crosscut illustrating preferential pyrrhotite replacement in the garnet-grunerite unit to the left, compared to the essentially barren chert-magnetite unit to the right. **d)** Photograph of a polished slab of typical Musselwhite ore showing intense silica flooding and pyrrhotite replacement of the iron formation. **e)** Photograph of a drill-core sample of very weakly altered garnet-grunerite iron formation. Abbreviations: f.g. = fine grained; Po = pyrrhotite; Qz = quartz.

(1986), the mineralized zones at Musselwhite show close spatial relationship with the D_2 deformation-related high-strain zones and adjacent lower pressure areas, such as F_2 fold hinge zones, supporting the syn-D_2 timing of Au mineralization, in association with sulphides such as pyrrhotite. Two end-members of ore can be distinguished: quartz-flooded zones with over 50% quartz and zones of strong pyrrhotite replacement (up to 40% pyrrhotite).

The 11780N Crosscut on level 770 exposes one of the PQD ore zones (Figs. 2b, 6a), which represents typical high-grade ore in the 4EA facies and its relationships with D_2 structures. A D_2 strain gradient, similar to that mapped at kilometre-scale between the West Antiform area and the mine area, is documented at decametre-scale underground and in drill core, where Au mineralization mainly occurs in high-strain zones, but likewise in adjacent low-pressure areas, such as fold hinges (Fig. 6a,b). Lithological control on sulphide precipitation and associated Au deposition is also evidenced by the contrast in intensity of pyrrhotite replacement and/or quartz-flooding between the garnet-grunerite facies (unit 4EA) and the chert-magnetite facies (unit 4B) of the iron formation (Fig. 6c). Ore-grade mineralization in chert-magnetite iron formation only occurs in zones of high strain, intense transposition, and that contain numerous fault-fill laminated quartz-pyrrhotite veins.

Typical Au ore in the garnet-grunerite iron formation (Fig. 6d) mainly comprises smoky grey to black quartz veins and/or quartz flooding with pyrrhotite and iron carbonate. Pyrrhotite is the dominant sulphide associated with Au mineralization. Chalcopyrite is very rarely present in hand samples. Arsenopyrite is also only locally present, and does not correlate with elevated Au grades. In garnet-grunerite layers, pyrrhotite occurs as very fine-grained aggregates along foliation planes and in pressure shadows and filling fractures of coarse-grained dark red almandine porphyroblasts. Boudinaged chert bands, quartz veins, or quartz-flooded layers contain dark green, fine-grained amphibole, biotite, and local clinopyroxene, likely hedenbergite.

Silicate minerals, such as garnet, grunerite or ferrotschermakite, and biotite are found in both regional metamorphic and ore-related mineral assemblages. Documentation of the different mineral textural relationships is critical to understanding the series of event that occurred. In this regard, garnet is a particularly important phase, as it is present in many lithologies and in various textural contexts (Fig. 7a). Differences between proximal and distal Au mineralization are partly illustrated in garnet textures. For example, the distal, least altered 4EA facies (Fig. 6e) comprises anhedral to subhedral almandine garnet, whereas typical ore contains coarse-grained, subhedral to euhedral, red almandine garnets (Fig. 6d).

Geostatistical analysis of the lithogeochemical data (e.g. binary and ternary plots, principal component analysis (PCA), correlation coefficient calculations) shows that Au is associated with Ag, Se, Te, and Cu, in addition to total-sulfur and loss-on-ignition components (Fig. 7b,c). The weaker correlation of CaO and CO_2, compared to an average greenstone-hosted orogenic deposit (Dubé and Gosselin, 2007), may denote the overprint of Au-bearing structures by calcite-rich structures, which were documented in underground mapping and in drill-core analyses. As proposed by Davies et al. (1982), CO_2/CaO and CO_2/CaO+MgO molar ratios will be used to investigate the carbonate-alteration intensity, as these ratios take into account the availability of Ca and Mg in the altered rock protolith. The absence of As (as well as Sb, Bi, and Pb) in the trace metals associated with Au is noteworthy as it is usually abundant in orogenic Au deposits (Pitcairn et al., 2006; Dubé and Gosselin, 2007). The distinct, isolated signature of SiO_2 suggests that multiple parameters have influenced its distribution in the iron formation (primary chert, barren early quartz vein, Au-bearing silica-flooding, etc.).

DISCUSSION

Stratigraphy and Structure

Detailed surface mapping in the Musselwhite area reveals that early (D_1) deformation had a major influence on the geometry and regional distribution of prospective BIF horizons. Tight to isoclinal F_1 folds are refolded, and locally obliterated by D_2 folds and fabrics, which dominate the regional structural pattern. The presence of local metric to decametric F_1 folds suggests they occur at regional-scale. New U-Pb geochronology (Fig. 4; McNicoll et al., 2013) indicates that unit 6 and unit 4F of the Northern BIF are both <2967 Ma, and the structurally overlying felsic tuff (Avol unit) of the South Rim assemblage yielded an age of 2978.7 Ma. Coupled with regional geological data, this data confirms that the mine sequence is overturned and occurs along the northern overturned limb of a kilometre-scale F_1 fold, with an inferred axial plane located along Zeemel Lake (Fig. 2a). New U-Pb isotope dilution thermal ionization mass spectrometry (ID-TIMS) geochronology results have also uncovered a ca. 60 to 110 Ma age difference between the OMA (<2967 to >2909.4 Ma) and the adjacent ZHA (<2853 Ma) in the mine stratigraphic succession (Fig. 4; McNicoll et al., 2013, submitted). Drill-core descriptions show this major gap or boundary is marked by increased strain intensity and carbonate alteration. Regional mapping (Fig. 2) suggests that this sheared contact likely delineates an early, D_1 thrust fault, which

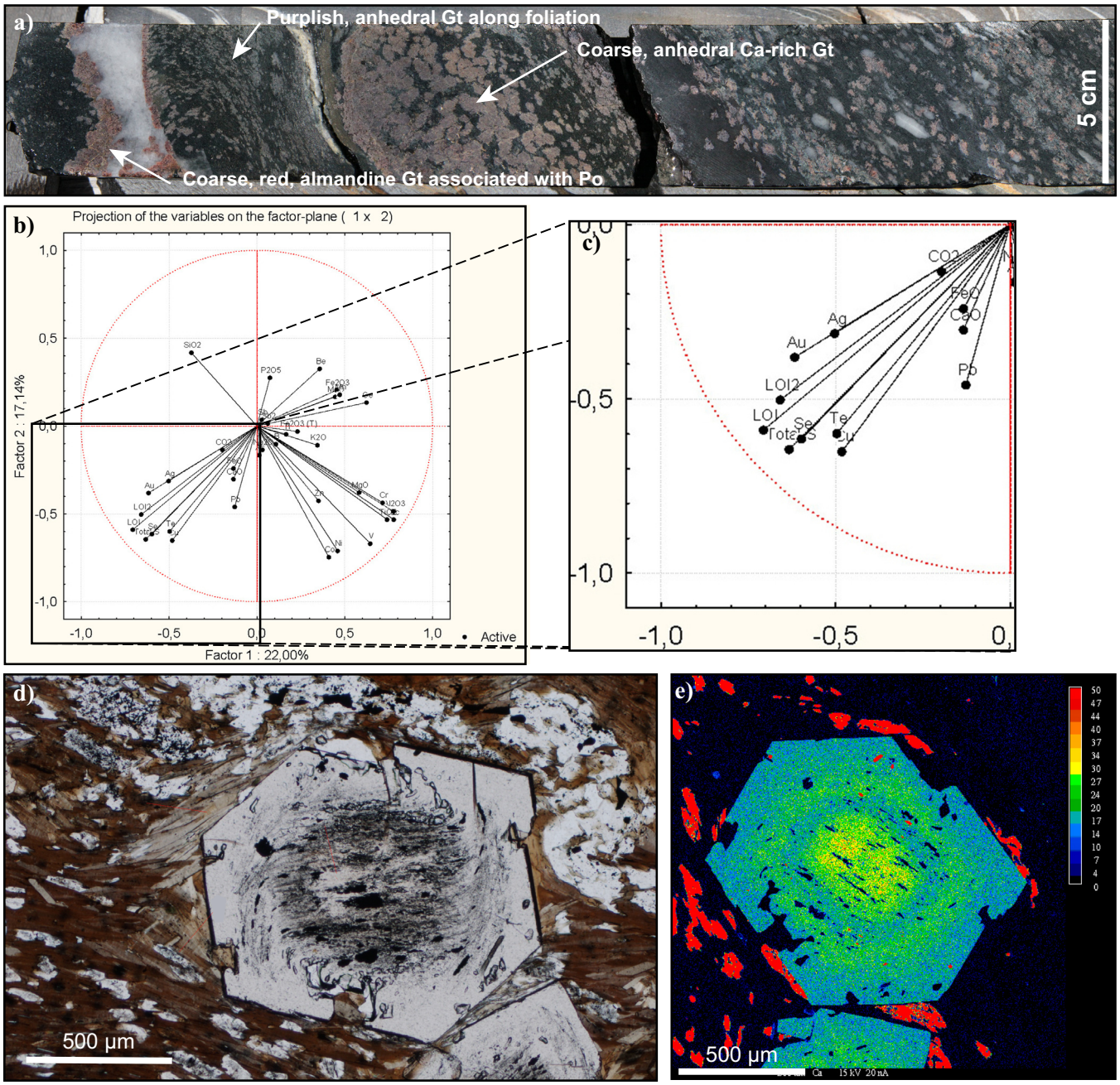

Figure 7. a) Photograph of drill-core sample containing three types of garnet (Gt): fine-grained, anhedral to subhedral, pale purple almandine distributed along the main foliation; coarse, subhedral, red almandine associated with pyrrhotite (po) in a quartz-dominated vein; and coarse, anhedral, pink to orange almandine associated with a calcite-rich veinlet. **b).** Principal component analysis (PCA) diagram for major elements and trace metals in the garnet-grunerite iron formation samples (4EA) using factors 1 and 2. **c)** Close-up of (b) showing the distinct association of trace metals with Au and S. **d)** Microphotograph of a garnet porphyroblast with a core containing folded inclusion trails marking an early fabric. **e)** Microprobe map of CaO content (percent) of the same garnet porphyroblast, note the halos of CaO enrichment concomitant with changes in orientation of inclusion trails.

may have reactivated a pre-existing unconformity.

The D_2 deformation is younger than 2846 Ma, which is the maximum age of the deformed ZHA (McNicoll et al., 2013). The D_2 deformation also deforms the margins of the 2870–2850 Ma North Caribou pluton and the 2860–2840 Ma Schade Lake gneissic complex (Breaks et al., 2001; Fig. 1). Competency contrast with the enclosed supracrustal rocks have induced strain partitioning during D_2 deformation and, thus, influenced the distribution and geometry of the BIF units during Au mineralization.

Recent geochronological work along the major shear zones of the area (Kelly et al., 2015) suggests that major faulting at ca. 2.75 to 2.71 Ga was followed by transpressive shear at ca. 2.60 to 2.56 Ga, and by late reactivation of pre-existing fault zones (e.g. Markop

shear zone: Fig. 1), occurring as late as 2.45 Ga. Field observations suggest this late reactivation event could correspond to the D_3 features that have been mapped in the present study area.

Mineralization and Alteration

Iron formations are extremely reactive to S-bearing fluids, thus Fe and S tend to combine to form pyrrhotite, which is the most abundant Au-associated sulphide at Musselwhite. The abundance of ore-related pyrrhotite at Musselwhite may originate from the metamorphic recrystallization of pyrite to pyrrhotite (Tomkins, 2010) or, more likely, because increasing metamorphic conditions favoured the crystallization of pyrrhotite during Au mineralization. Given the empirical correlation between pyrrhotite content and Au grade (1% pyrrhotite ≈ 1 ppm Au; W. McLeod, pers. comm., 2011) and the high Pearson correlation coefficient between Au and S in preliminary geochemical data (0.5–0.8), Au was most probably transported as thiocomplexes ($Au(HS)_2^-$ or $AuHS_0$; e.g. McCuaig and Kerrich, 1998), and released during pyrrhotite crystallization. In the silicate facies of the iron formation (unit 4EA), Fe is thought to have been derived from the breakdown of grunerite into Ca-amphibole, likely ferro-tschermakite and actinolite, which contain less Fe. In the adjacent clastic chert-magnetite facies of the iron formation (unit 4Bc), the large amount of magnetite provides a significant source of Fe to form pyrrhotite along with Fe-carbonate, especially ankerite. These replacements are interpreted to reflect the CaO enrichment usually associated with the alteration halo of orogenic Au mineralization (Dubé and Gosselin, 2007 and references therein).

The successive development of grunerite, almandine, and clinopyroxene indicate lower to mid-amphibolite-facies metamorphic conditions in iron formation (Klein, 2005). Relative timing of mineralization is best constrained by relationships with the structure and metamorphic paragenesis. Euhedral garnet porphyroblasts, e.g., at the Esker Docks exposure, have cores indicating a pre-existing foliation (S_1 or early S_2; Fig. 7d), and are characterized by an intermediate corona that recorded a subsequent progressive deformation, probably D_2, associated with increased Ca content (Fig. 7e). Euhedral outer rims that overprint the main S_2 foliation indicate late to post-D_2 growth and suggest that peak metamorphic temperature occurred during the latter stages of D_2 deformation. In high-grade zones, Au is present as inclusions and as fracture-filling in garnet porphyroblasts or in pressure-shadows developed along garnet crystals, suggesting that Au mineralization, or its local remobilization, occurred after the initiation of garnet porphyroblast crystallization during active D_2 deformation.

Stable isotope data (Isaac, 2008), coupled with the trace element signature of Au mineralization (e.g. Ag, Cu, Se, Te; Fig. 7b,c), suggest that the Musselwhite deposit is compatible with the metamorphic end-member of the greenstone-hosted Au deposit group (i.e. ore-fluids that are mainly of metamorphic origin; cf. Dubé and Gosselin, 2007). Syn-D_2 major compression (flattening-dominated) of rheologically contrasting units in the mine area induced the development of discrete subvertical high-strain zones in the iron formation, along with intense folding. Preliminary interpretations of our observations and data suggest that Au-bearing fluids were channelled into the high-strain zones and also migrated into adjacent F_2 fold hinge zones, which constituted areas of lower pressure suitable for trapping gold mineralization. Moreover, the Fe-rich, highly reactive 4EA NIF unit caused the destabilization of the Au-transporting agents and facilitated Au precipitation (a chemical trap). So, the rheological contrasts between the NIF and the surrounding igneous rocks (lithological/stratigraphic trap), at amphibolite-facies conditions, and its high-iron content (a chemical trap) explains the preferential deposition of Au in the iron formation at Musselwhite.

Biczok et al. (2012) published Sm-Nd isotopic analyses on several euhedral, red, almandine garnets spatially associated with Au that yielded a preferred age of 2690 ± 9 Ma, which is interpreted as the age of Au mineralization at Musselwhite. Newly acquired U-Pb SHRIMP (Sensitive High Resolution Ion Microprobe) in situ analyses of monazite grains in the garnet-biotite schist (unit 4F), conducted within this project, give a preliminary age of 2666 ± 6 Ma, which is interpreted to represent the timing of peak metamorphism. Analyzed monazite grains were located in the biotite matrix and in inclusion-poor outer rims of garnet porphyroblasts that appear to have grown during late- to slightly post-D_2 deformation, similar to the outermost rim of the garnet in Figure 6d. Given this relationship and the strong link between metamorphic paragenesis and mineralization, this monazite age is interpreted as a minimum age for the main Au mineralization event. As the D_2 deformation is younger than 2846 Ma, the bulk of the gold mineralization is bracketed between 2846 and 2666 Ma.

IMPLICATIONS FOR EXPLORATION

The interpretation of kilometre-scale F_1 folding in the Opapimiskan Lake area has implications for the location and geometry of prospective iron formation horizons and may thus provide new regional exploration targets. A strong D_2 strain gradient is documented in supracrustal rocks of the North Caribou greenstone belt, increasing northeastward toward the tight F_2 fold hosting the Musselwhite deposit and culminating at the

tectonic contact with the Shade Lake gneissic complex of the Island Lake Domain. This major first-order tectonic boundary, the early stage unconformity and/or thrust fault at the contact between the Opapimiskan-Markop and the adjacent Zeemel-Heaton assemblages, and the recently documented presence of polymictic conglomerate in the upper stratigraphic sequence (Fig. 1) are all critical features typically found in greenstone-hosted orogenic Au districts (e.g. Goldfarb et al., 2005; Robert et al., 2005; Dubé and Gosselin, 2007, Bleeker, 2012 and references therein). They provide targets for exploration throughout the greenstone belt, especially where associated with second-order D_2 structures affecting highly reactive BIF.

FUTURE WORK

Variations in mineral assemblages and chemistry between distal (barren) and proximal (mineralized) iron formation facies characterize the hydrothermal footprint of the deposit. Garnet porphyroblasts are present in various lithologies (Fig. 4a) and display multiple growth phases (Fig. 7d,e). Future work will include additional petrographic description to investigate relationships and timing of mineral growth. Mineral chemistry will also be used to better understand individual element variations in whole rock lithogeochemical data, such as the decoupling between Mn that is contained in the garnet cores, and thus isolated from subsequent hydrothermal events, and Mg that is contained in the matrix amphibole.

Ongoing spatial analysis and integration of the lithogeochemical database will allow characterization of the distribution and relative timing of the various types of alteration present at Musselwhite. Targeted LA-ICP-MS elemental mapping of sulphide minerals (cf. Cabri and Jackson, 2011) from samples of the ZHA will also document the evolution and distribution of trace metals during metamorphism and deformation, as was completed previously on pyrite nodules from an argillite unit of the West Antiform area (Jackson et al., 2013).

Multiple occurrences of polymictic conglomerates within the ZHA have been recently documented and subsequently sampled for geochronology study. The results will need to be interpreted in light of the geological setting of each outcrop and will likely impact the current stratigraphic model in the Opapimiskan Lake area.

ACKNOWLEDGEMENTS

This report emanates from the ongoing Ph.D. thesis undertaken by the first author (W. Oswald) at the Institut national de la recherche scientifique (INRS-ETE), as part of the Targeted Geoscience Initiative 4 (Lode Gold project) of Natural Resources Canada. Additional support is provided by Natural Sciences and Engineering Research Council of Canada (NSERC), Fonds de recherche du Québec (FRQNT) and Goldcorp Inc., through the Industrial Innovation Scholarship program (BMP/IIS) to the first author (W. Oswald). We sincerely thank Goldcorp Inc. Musselwhite Mine for access to the property, to drill core, and various data sets, and for chartered transport and accommodation. Rohan Millar, Jim Edwards, and Bill McLeod, as well as the entire production and exploration team of the Musselwhite Mine, are acknowledged for their time, operational support, interest in this project, and for sharing their unique knowledge of the deposit. The project has also benefited from the collaboration and discussions with Phil Thurston from the Laurentian University, Dave Schneider, Keiko Hattori, Colter Kelly, Emilie Gagnon, and Octavia Bath from the University of Ottawa and Wouter Bleeker of the GSC Ottawa. The manuscript has strongly benefited from Phil Thurston's constructive comments and suggestions.

REFERENCES

Baldwin, G.J., 2011. The sedimentology and geochemistry of banded iron formations of the Deloro assemblage, Barlett Dome area, Abitibi greenstone belt, Ontario, Canada: Implications for BIF deposition and greenstone belt formation; M.Sc. Thesis, Laurentian University, Sudbury, Ontario, 121 p.

Biczok, J., Hollings, P., Klipfel, P., Heaman, L., Maas, R., Hamilton, M., Kamo, S., and Friedman, R., 2012. Geochronology of the North Caribou greenstone belt, Superior Province Canada: Implications for tectonic history and gold mineralization at the Musselwhite mine; Precambrian Research, v. 192-195, p. 209−230.

Bleeker, W., 2012. Targeted Geoscience Initiative 4. Lode gold deposits in ancient deformed and metamorphosed terranes: The role of extension in the formation of Timiskaming basins and large gold deposits, Abitibi greenstone belt—A Discussion, *In:* Summary of field work and other activities 2012; Ontario Geological Survey, Open File Report 6280, p.47-1 to 47-12.

Breaks, F.W., Bartlett, J.R., Osmani, I.A., Finamore, P.F., and Wallace, H., 1985. Opapimiskan lake project: Precambrian and Quaternary geology of the North Caribou Lake area, district of Kenora, Patricia Portion, *In:* Summary of field work and other activities 1985; Ontario Geological Survey, Miscellaneous Paper 126, p. 268–276.

Breaks, F.W. and Bartlett, J.R., 1991. Geology of the Eyapamikama Lake Area; Ontario Geological Survey, Open File Report 5792, 132 p.

Breaks, F.W., Bartlett, J.R., de Kemp, E.A., and Osmani, I.A., 1991. Geology of the Doubtful-Akow lakes area, district of Kenora; Ontario Geological Survey, Open File Report 5795, 131 p.

Breaks, F.W., Osmani, I.A., and de Kemp, E.A., 2001. Geology of the North Caribou Lake area, northwestern Ontario; Ontario Geological Survey, Open File Report 6023, 80 p.

Cabri, L.J. and Jackson, S.E., 2011. New developments in characterization of sulphide refractory gold ores, In: Proceedings of the 50th Conference of Metallurgists, October 2-5, 2011, Montreal, Quebec, p. 51–62.

Couture, G., 1995. Stratigraphy, lithology, structural history and grade distribution of the Musselwhite gold prospect; unpublished report for Placer Dome Canada Limited, 102 p.

Cox, S. F., Knackstedt, M.A., and Braun, J., 2001. Principles of structural control on permeability and fluid flow in hydrothermal systems; Reviews in Economic Geology, v. 14, p. 1–24.

Davies, J.F., Whitehead, R.E.S., Cameron, R.A., and Duff, D., 1982. Regional and local patterns of CO_2-K-Rb-As alteration: A guide to gold in the Timmins area, *In:* Geology of Canadian Gold Deposits (ed.) R.W. Hodder and W. Petruk; Canadian Institute of Mining and Metallurgy, Special Volume 24, p.130–143.

Dubé, B., Mercier-Langevin, P., Castonguay, S., McNicoll, V.J., Pehrsson, S.J., Bleeker, W., Schetselaar, E.M., and Jackson, S., 2011. Targeted Geoscience Initiative 4. Lode gold deposits in ancient deformed and metamorphosed terranes – footprints and exploration implications: a preliminary overview of themes, objectives and targeted areas, *In:* Summary of field work and other activities 2011; Ontario Geological Survey, Open File Report 6270, p. 38-1 to 38-10.

Dubé, B. and Gosselin, P., 2007. Greenstone-hosted quartz-carbonate vein deposits, *In:* Mineral Deposits of Canada: A Synthesis of Major Deposit Types, District Metallogeny, the Evolution of Geological Provinces, and Exploration Methods, (ed.) W.D. Goodfellow; Geological Association of Canada, Mineral Deposits Division, Special Publication, No. 5, p. 49–73.

Duff, J., 2014. A geochemical and isotopic investigation of metasedimentary rocks from the North Caribou greenstone belt, western Superior Province, Canada; M.Sc. Thesis, University of Ottawa, Ottawa, Ontario, Canada, 189 p.

Goldfarb, R.J., Baker, T., Dubé, B., Groves, D.I., Hart C.J.R., and Gosselin, P., 2005. Distribution, character, and genesis of gold deposits in metamorphic terranes, *In:* Economic Geology 100th Anniversary Volume, (ed.) J.W. Hedenquist, J.F.H. Thompson, R.J. Goldfarb, and J.P. Richards; Society of Economic Geology, p. 407–450.

Gourcerol, B., Thurston, P.C., Kontak, D.J., and Côté-Mantha, O., 2014. Interpretations and implications of preliminary LA ICP-MS analysis of chert for the origin of geochemical signatures in banded-iron-formations from the Meadowbank gold deposit, western Churchill Province, Nunavut; Geological Survey of Canada, Current Research 2013-20, 22 p. doi:10.4095/293129

Gourcerol, B., Thurston, P.C., Kontak, D.J., Côté-Mantha, O., and Biczok, J., 2015. Depositional setting of Algoma-type banded iron formation from the Meadowbank, Meliadine and Musselwhite gold deposits, *In:* Targeted Geoscience Initiative 4: Contributions to the understanding of Precambrian lode gold deposits and implications for exploration, (ed.) B. Dubé and P. Mercier-Langevin; Geological Survey of Canada, Open File 7852, p. 55–68.

Hall, R.S. and Rigg, D.M., 1986. Geology of the West Anticline Zone, Musselwhite Prospect, Opapimiskan Lake, Ontario, Canada, *In:* Proceedings of Gold '86 Symposium, September 28th to October 1st, Toronto, Canada, p. 124–136.

Hollings, P. and Kerrich, R., 1999. Trace element systematics of ultramafic and mafic volcanic rocks from the 3 Ga North Caribou greenstone belt, northwestern Superior Province; Precambrian Research, v. 93, p. 257–279.

Isaac, C., 2008. Stable isotope (N, O, H) geochemistry, petrology and compositions of biotite of the Musselwhite Mine, Ontario: implications for mineralization; M.Sc. Thesis, Lakehead University, Thunder Bay, Ontario, 133 p.

Jackson S., Gao, J., and Dubé, B., 2013. Nouveaux développements applicables à l'analyse des éléments en traces dans les dépôts de minéraux et à la cartographie utilisée pour la recherche et l'exploration des gisements de minerai : exemples de gisements d'or du Québec et de l'Ontario, *In:* Résumés des conférences et des photoprésentations, Québec Mines, 11-14 Novembre, 2013, Québec, Québec, p. 16.

James, H.L., 1954. Sedimentary facies of iron-formations; Economic Geology, v. 49, p. 235–293.

Kalbfleisch, N., 2012. Crustal-scale shear zones recording 400 M.Y. of tectonic activity in the North Caribou greenstone belt, western Superior Province of Canada; M.Sc. Thesis, University of Ottawa, Ottawa, Ontario, 162 p.

Kamber, B.S., Greig A., and Collerson, K.D., 2005. A new estimate for the composition of weathered young upper continental crust from alluvial sediments, Queensland, Australia; Geochimica et Cosmochimica Acta, v. 69, p. 1041–1058.

Kelly, C.J. and Schneider, D.A., 2015. Insights into the timing of mineralization and metamorphism in the North Caribou greenstone belt, western Superior Province, *In:* Targeted Geoscience Initiative 4: Contributions to the understanding of Precambrian lode gold deposits and implications for exploration, (ed.) B. Dubé and P. Mercier-Langevin; Geological Survey of Canada, Open File 7852, p. 245–253.

Klein, C., 2005. Some Precambrian banded iron-formations (BIFs) from around the world: Their age, geologic setting, mineralogy, metamorphism, geochemistry, and origin; American Mineralogist, v. 90, p. 1473–1499.

McCuaig, C.T. and Kerrich, R., 1998. P-T-t-deformation-fluid characteristics of lode gold deposits: evidence from alteration systematics; Ore Geology Reviews, v. 12, p. 381–453.

McLean, T.J. and Barrett, W.H., 1993. Lithogeochemical techniques using immobile elements; Journal of Geochemical Exploration, v. 48, p. 109–133.

McNicoll, V., Dubé, B., Biczok, J., Castonguay, S., Oswald, W., Mercier-Langevin, P., Skulski, T., and Malo, M., 2013. The Musselwhite gold deposit, North Caribou greenstone belt, Ontario: new high-precision U-Pb ages and their impact on the geological and structural setting of the deposit, *In:* Program with Abstracts; Geological Association of Canada-Mineralogical Association of Canada joint annual meeting, May 22-24, 2013, Winnipeg, Manitoba, v. 36, p. 142.

McNicoll, V., Dubé, B., Castonguay, S., Oswald, W., Biczok, J., Mercier-Langevin, P., Skulski, T., and Malo, M., submitted. The world-class Musselwhite BIF-hosted gold deposit, Superior Province, Canada: new high-precision U-Pb geochronology and implications for the geological and structural setting of the deposit and gold exploration; Precambrian Research.

Moran, P., 2008. Lithogeochemistry of the Sedimentary Stratigraphy and Metosomatic Alteration in the Musselwhite Gold Deposit, North Caribou Lake Belt, Superior Province, Canada: Implications for Deposition and Mineralization: M.Sc. Thesis, Lakehead University, Thunder Bay, Ontario, 411 p.

Oswald, W., Dubé, B., Castonguay, S., McNicoll, V., Biczok, J., Mercier-Langevin, P., Malo, M., and Skulski, T., 2014a. New insights on the geological setting of the world-class Musselwhite gold deposit, Superior Province, northwestern Ontario, *In:* Program with Abstracts; Geological Association of Canada-Mineralogical Association of Canada joint annual meeting, May 21-23, 2014, v. 37, p. 311.

Oswald, W., Dubé, B., Castonguay, S., McNicoll, V., Biczok, J., Mercier-Langevin, P., Malo, M., and Skulski, T., 2014b. New insights on the structural and geological setting of the world-class Musselwhite gold deposit, Superior Province, Northwestern Ontario; Geological Survey of Canada Open File 7633, 1 poster.

Oswald, W, Castonguay, S., Dubé, B., Mercier-Langevin, P., Malo, M., Biczok, J., and McNicoll, V., 2014c. Targeted Geoscience Initiative 4. Lode gold deposits in ancient deformed and metamorphosed terranes: detailed mapping of key stripped outcrops in the Musselwhite Mine area, Northwestern Ontario, and implications for the geological and structural setting of the gold

mineralization, *In:* Summary of Field Work and other Activities 2014; Ontario Geological Survey, Open File Report 6300, p. 42-1 to 42-15.

Percival J.A., 2007. Geology and metallogeny of the Superior Province, Canada, *In:* Mineral Deposits of Canada: A Synthesis of Major Deposit Types, District Metallogeny, the Evolution of Geological Provinces, and Exploration Methods, (ed.) W.D. Goodfellow; Geological Association of Canada, Mineral Deposits Division, Special Publication No. 5, p. 903–928.

Piroshco, D.W., Breaks, F.W., and Osmani, I.A., 1989. The geology of gold prospects in the North Caribou Lake greenstone belt, district of Kenora, northwestern Ontario; Ontario Geological Survey, Open File Report 5698, 94 p.

Pitcairn, I., Damon, A., and Teagle, H., 2006. Sources of metals and fluids in orogenic gold deposits: Insights from the Otago and Alpine schists, New Zealand; Economic Geology, v. 101, p. 1525–1546.

Rayner, N., and Stott, G.M., 2005. Discrimination of Archean domains in the Sachigo Subprovince: a progress report on the geochronology, *In:* Summary of Field Work and other Activities 2005, Ontario Geological Survey, Open File Report 6172, p. 10-1 to 10-21.

Robert, F., Poulsen, K.H., Cassidy, K.F., and Hodgson, C.J., 2005. Gold metallogeny of the Superior and Yilgarn cratons, *In:* Economic Geology 100th Anniversary Volume, (ed.) J.W. Hedenquist, J.F.H. Thompson, R.J. Goldfarb, and J.P. Richards; Society of Economic Geology, p. 1001–1033.

Ross, P. S. and Bédard, J. H., 2009. Magmatic affinity of modern and ancient subalkaline volcanic rocks determined from trace-element discriminant diagrams; Canadian Journal of Earth Sciences, v. 46, p. 823–839.

Stott, G.M., Corkery, M.T., Percival, J.A., Simard, M., and Goutier, J., 2010. A revised terrane subdivision of the Superior Province, *In:* Summary of Field Work and other Activities 2010; Ontario Geological Survey, Open File Report 6260, p. 20-1 to 20-10.

Sun, S.-S. and McDonough, W.F., 1989. Chemical and isotope systematics of oceanic basalts: implications for mantle composition and processes, *In:* Magmatism in the Ocean Basins, (ed.) A.D. Saunders and M.J. Norry; Geological Society, London, Special Publication No. 42, p. 313–345.

Thurston, P., Osmani, I. and Stone, D., 1991. Northwestern Superior Province: review and terrane analysis, *In:* Geology of Ontario, Special Volume 4, Part 1, (ed.) P.C. Thurston, H.R. Williams, R.H. Sutcliffe, and G.M. Stott; Ontario Geological Survey, p. 80–142.

Tomkins, A., 2010. Windows of metamorphic sulfur liberation in the crust: Implications for gold deposit genesis; Geochimica et Cosmochimica Acta; v. 74, p. 3246–3259.

Van Lankvelt, A., 2013. Protracted magmatism within the North Caribou Terrane, Superior Province: petrology, geochronology, and geochemistry of Meso- to Neoarchean TTG suites; M.Sc. thesis, University of Ottawa, Ottawa, Ontario, 204 p.